

Article

# Preparation of PP-g-(AA-MAH) Fibers Using Suspension Grafting and Melt-Blown Spinning and its Adsorption for Aniline

Zhouyang Lian \*, Yiyang Xu, Jie Zuo, Hui Qian, Zhengwei Luo and Wuji Wei 

School of Environmental Science and Engineering, Nanjing Tech University, Nanjing 211816, China; YI\_AMARIS@163.COM (Y.X.); zuojieyx@163.com (J.Z.); qianhui@fiberglasschina.com (H.Q.); luozw1989@163.com (Z.L.); wjwei@njtech.edu.cn (W.W.)

\* Correspondence: lianzy@njtech.edu.cn

Received: 26 August 2020; Accepted: 18 September 2020; Published: 22 September 2020



**Abstract:** This paper uses polypropylene (PP) as the matrix and acrylic acid (AA) and maleic anhydride (MAH) as functional monomers to prepare PP-g-(AA-MAH) fibers by suspension grafting and melt-blown spinning technology that are easy to industrially scale-up. The fibers can be used to adsorb aniline. Results showed that the grafting ratio reached the maximum of 12.47%. The corresponding optimal conditions were grafting time of 3 h, AA: MAH = 0.75, total monomer content of 55%, benzoyl peroxide 1.4%, xylene concentration of 6 mL/g PP, and deionized water content of 8 mL/g PP. Owing to its good fluidity and thermal stability, the product of suspension grafting can be used for melt-blown spinning. Infrared spectroscopic and nuclear magnetic resonance spectroscopic analyses indicated that AA and MAH were successfully grafted onto PP fibers. After grafting, the hydrophilicity of PP-g-(AA-MAH) fiber increased. Therefore, it had higher absorptivity for aniline and the adsorption capacity could reach 42.2 mg/g at 45 min and pH = 7. Moreover, the PP-g-(AA-MAH) fibers showed good regeneration performance.

**Keywords:** polypropylene; suspension grafting; melt-blown spinning; adsorption; aniline

## 1. Introduction

Water discharged from industrial activities, if left untreated or not treated to the proper standard, inevitably causes water pollution, which is one of the major environmental issues of the day [1,2]. Aniline is one of the common organic compounds used as an intermediate in chemical industry, and hence its market demand has risen sharply [3–5]. This provides more channels for aniline to enter water bodies, thus causing environmental pollution. Since aniline does not readily undergo degradation, it accumulates in the environment. Moreover, being a carcinogenic, teratogenic, mutagenic, and highly toxic substance, aniline has a severely high risk of causing potential damage to the environment and organisms [6–8]. Therefore, aniline has been included in the list of preferentially controlled pollutants by Minister of Ecology and Environment of China, the United States Environmental Protection Agency, European Chemicals Agency, and other agencies [9–11].

At present, treatment methods for aniline-containing wastewaters mainly include advanced oxidation [12,13], membrane separation [14,15], extraction [16,17], biological methods [18], and adsorption methods [19–22]. Among them, the adsorption method that uses the interactions between adsorbent and adsorbate to remove pollutants from wastewater has attracted the attention of researchers, because of its simple operation, fast processing, and resourceful recovery [23]. Especially for treating sudden incidents of water pollution, adsorption method is considered as the first choice, owing to its high efficiency. Therefore, the development of adsorbents using a wide range of raw

materials, at low price, and achieving strong adsorption capacity through simple post-adsorption treatment of aniline wastewater has become the focus of research [24].

Polypropylene (PP) is acid- and alkali-resistant, very common material, cheap, and easy to process. After PP is spun by melt-blowing into fibers, it forms a three-dimensional network structure, with smaller mono-filament diameter, higher porosity, and larger specific surface area [25–27]. Therefore, it has been widely used as a matrix fiber. However, since PP is non-polar in nature, it does not possess polar and reactive groups along its molecular chains, which limits its ability to adsorb pollutants from wastewaters [28]. Our research group has been actively involved in the preparation of functionalized PP fibers with special properties through grafting, chemical modification, and other methods [29–31].

Suspension grafting [32] is a new, environment-friendly, and easy-to-industrialize method for grafting modification. This method usually employs water as the dispersion medium and polymer particles as the dispersed phase. It forms a suspension system, under the action of shear force provided by mechanical stirring. Each suspended polymer particle can be regarded as an independent “reaction bed”. Within this “reaction bed”, the functional monomers undergo graft polymerization under the action of initiators. This polymerization method has advantages of high reaction efficiency, few side reactions, and simple post-processing of products. Li et al. [33] prepared PP-g-PMMA with water as the dispersant and dibenzoyl peroxide as the initiator using the suspension grafting method. The addition of a second monomer, styrene, increased the grafting ratio of monomer to 24.5%. This indicated an effective improvement in the compatibility of PP/ASA mixture.

In this study, the amorphous region of PP was first expanded by quenching treatment, and then functional monomers like acrylic acid (AA) and maleic anhydride (MAH) were grafted onto the surface of PP by suspension grafting. Finally, the PP-g-(AA-MAH) fibers were prepared by melt-blown spinning technology. The adsorption and regeneration performance of PP-g-(AA-MAH) fibers for aniline in aqueous solution were investigated.

## 2. Experimental

### 2.1. Experimental Materials

PP resin especially for the melt-blown process was provided by Shanghai Expert New Material Co. Ltd. (Shanghai, China). Other chemical reagents, such as AA, MAH, xylene, benzoyl peroxide (BPO), acetone, absolute ethanol, sodium hydroxide, hydrochloric acid, etc. were all analytically pure and commercially available.

### 2.2. Preparation of PP-g-(AA-MAH) Fibers

A certain amount of PP resin and xylene were charged into a magnetically stirred reactor and the temperature was raised to 140 °C under stirring. Then, a certain amount of deionized water was rapidly pumped at normal temperature into the reactor to cool down the temperature of the reaction mixture. After this, the temperature of the reactor was maintained at 90 °C and then the mixture was allowed to swell for 30 min. Then, the monomers AA and MAH and BPO initiator were added to the reaction kettle through the high-pressure feed port and graft polymerization was carried out for a certain period of time under strong stirring. The obtained products were washed with deionized water and acetone to remove unreacted monomers and homopolymers. The washed product was dried and then passed through a melt-blown spinning machine [34] to obtain PP-g-(AA-MAH) fibers.

### 2.3. Calculation of Grafting Ratio

PP-g-(AA-MAH) fibers (0.5 g) were placed in a 250 mL round-bottom flask. Xylene (100 mL) and sodium hydroxide-ethanol solution (0.05 mol/L, 30 mL) were added in succession. The mixture was allowed to boil at 120 °C for 30 min. After the solution was cooled to room temperature, 3–5 drops of thymol blue indicator was added and then the mixture was titrated with hydrochloric acid-isopropanol

solution (0.05 mol/L) until the blue color just disappeared. The ungrafted PP fibers were used as the blank sample for comparison. The grafting ratio was calculated as follows:

$$G_p\% = \frac{(V_0 - V_1) \times C \times (98.06 + 72.06)}{3 \times m} \times 100\% \quad (1)$$

where  $G_p(\%)$  denotes the grafting ratio;  $V_0(L)$  and  $V_1(L)$  represent the volumes of HCl-isopropanol solution consumed to titrate PP fibers and PP-g-(AA-MAH) fibers, respectively;  $C(\text{mol/L})$  denotes the concentration of HCl-isopropanol solution;  $m(\text{g})$  denotes the mass of the fiber sample; 98.06 g/mol and 72.06 g/mol are the molar masses of MAH and AA, respectively.

#### 2.4. Characterization Methods

An X-ray diffractometer (X'TRA, ThermoFisher Scientific, Waltham, MA, USA) was used to characterize the crystal structures of sample before and after quenching. The fluidity and thermal stability of the suspension grafting product were studied by melt indexer (RL-Z1B1, SRD, Shanghai, China) and thermal analyzer (Pyris 1 DSC, PerKinElmer, Waltham, MA, USA), respectively. The functional groups of the modified fibers were analyzed using a Fourier transform infrared spectrometer (Nexus 670, Nicolet, Waltham, MA, USA) and nuclear magnetic resonance spectrometer (DRX500, BRUKER, Karlsruhe, Germany).

#### 2.5. Hydrophilicity of PP-g-(AA-MAH) Fiber

The Washburn equation [35] can determine the contact angle of a dynamic liquid by measuring the speed at which the liquid penetrates into the filled powder (Equation (2)). However, the penetration height of wetting liquid is difficult to determine. As the penetration height changes, the air in the capillary tube gets compressed and the air pressure increases [36]. Therefore, Equation (2) can be revised by the relationship between osmotic pressure and height and Equation (3) is obtained.

Let  $K_\theta = \frac{\beta\gamma_{LV} \cos \theta}{\eta}$ ,  $K_\theta$  can be obtained from the linear relationship between  $(\Delta P)^2$  and  $t$ .

In this study, the water contact angle of degreased cotton with good hydrophilicity was set to 0, that is, when  $\theta = 0$ , then the equation becomes  $K_0 = \frac{\beta\gamma_{LV}}{\eta}$ . Since the bulk densities of all the test samples was almost the same and deionized water was used as the wetting liquid, the  $\beta$ ,  $\eta$ , and  $\gamma_{LV}$  values of the test samples were approximately the same. Due to these similarities, Equation (4) can be obtained for calculating the water contact angle on the surface of tested fiber. The schematic diagram of the self-made device is shown in Figure 1.

$$h^2 = \frac{R_{eff} \gamma_{LV} \cos \theta}{2\eta} t \quad (2)$$

$$(\Delta P)^2 = \frac{\beta\gamma_{LV} \cos \theta}{\eta} t \quad (3)$$

$$\theta = \arccos\left(\frac{K_\theta \eta}{\beta\gamma_{LV}}\right) = \arccos\left(\frac{K_\theta}{K_0}\right) \quad (4)$$

where  $h$  denotes the penetration height of the wetting liquid in time  $t$ ;  $R_{eff}$  denotes the effective capillary radius;  $\gamma_{LV}$  denotes the surface tension of the wetting liquid;  $\theta$  denotes the water contact angle;  $\eta$  denotes the viscosity of the wetting liquid;  $t$  denotes the penetration time;  $\Delta P$  denotes the change in osmotic pressure, and  $\beta$  denotes the parameters related to the stacking mode of the stacked bed.

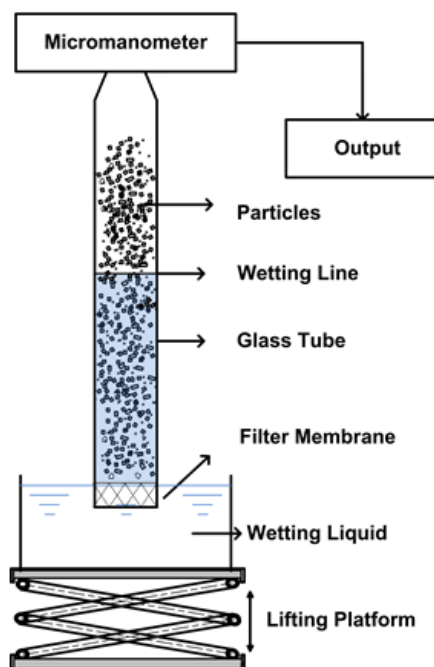


Figure 1. The schematic diagram of the self-made device.

2.6. Adsorption and Desorption of Aniline by PP-g-(AA-MAH) Fiber

Ten portions of potassium nitrate (0.01 mol/L, 20 mL) were taken and each portion was transferred to a conical flask. It was purged with N<sub>2</sub> to remove CO<sub>2</sub>. The pH was adjusted to values between 2–10 using 0.01 mol/L HCl and 0.01 mol/L NaOH solutions. The pH value was recorded as pH<sub>0</sub>. Then, PP-g-(AA-MAH) fibers (0.2 g) was added to the conical flask, flask was sealed, and shaken for 36 h in a water bath at room temperature. Thereafter, the fibers were taken out and the pH value of solution was measured, which was denoted as pH<sub>f</sub>. The pH<sub>0</sub> values were plotted along the X axis and pH<sub>0</sub>-pH<sub>f</sub> values along the Y axis, to fit a straight line. The point of intersection of the straight line and the X axis was recorded as the point of zero charge of the PP-g-(AA-MAH) fiber.

Deionized water was used to prepare a mono-contaminated solution containing a certain concentration of aniline and the pH value was adjusted with 0.01 mol/L HCl and 0.01 mol/L NaOH solutions. After adsorption at 25 °C under shaking, the fibers were taken out. After allowing to stand for 5 min, the aniline concentration was determined, and the adsorption capacity was calculated from equation.

$$Q = \frac{(C_0 - C_1)V}{m} \tag{5}$$

where *Q* (mg/g) denotes the adsorption capacity; *C*<sub>0</sub> (mg/L) and *C*<sub>1</sub> (mg/L) denote the concentrations of aniline in the solution before and after adsorption; *V* (L) denotes the volume of the solution; and *m* (g) is the mass of fiber as absorbent.

The adsorption kinetics were fitted with pseudo-first-order (Equation (6)) and pseudo-second-order (Equation (7)) models.

$$\ln(Q_e - Q_t) = \ln Q_e - K_1 t \tag{6}$$

$$\frac{t}{Q_t} = \frac{1}{K_2 Q_e^2} + \frac{t}{Q_e} \tag{7}$$

where *Q*<sub>*e*</sub> (mg/g) and *Q*<sub>*t*</sub> (mg/g) are the amount of adsorbed aniline at equilibrium and at an arbitrary time *t*(min), respectively; and *K*<sub>1</sub> (1/min) and *K*<sub>2</sub> (mg/g/min) are the pseudo-first-order and pseudo-second-order rate constants of adsorption, respectively.

The adsorption isotherm was analyzed with the Langmuir and Freundlich models:

$$\frac{C_e}{Q_e} = \frac{C_e}{Q_m} + \frac{1}{K_L Q_m} \quad (8)$$

$$\ln Q_e = \ln K_F + \frac{1}{n} \ln C_e \quad (9)$$

where  $C_e$  (mg/L) is the concentration of aniline in solution at equilibrium;  $Q_e$  (mg/g) is the equilibrium adsorption capacity;  $Q_m$  (mg/g) is the maximum adsorption capacity;  $K_L$  (L/mg) is the Langmuir constant;  $K_F$  (L/mg) is the Freundlich constant indicative of the adsorption capacity;  $n$  is a parameter related to the sorption intensity.

The adsorption-saturated PP-g-(AA-MAH) fiber was desorbed by shaking in 0.5 mol/L HCl solution for a certain period of time. The concentrations of aniline in the solution were measured at different times and the desorption ratios were calculated from Equation (10) [37].

$$D = \frac{CV}{mQ} \times 100\% \quad (10)$$

where  $D$  (%) denotes the desorption ratio;  $C$  denotes the concentration of aniline in the eluent (mg/L);  $Q$  is the adsorption capacity of the fiber (mg/g);  $V$  is the volume of the eluent (L), and  $m$  denotes mass of fiber (g).

### 3. Results and Discussion

#### 3.1. The Mechanism of Suspension Grafting Polymerization of Two Monomers

The schematic diagram of suspension grafting polymerization of AA and MAH monomers [29] is shown in Figures 2 and 3. In the suspension grafting reaction system, under the action of shear force provided by high-speed stirring, each PP resin particle swelled up and was surrounded by xylene. It dispersed into an independent “reaction bed” in deionized water as the dispersant. The grafting polymerization in each “reaction bed” mainly occurred in the amorphous regions of PP resin. In this study, PP resin was quenched before the graft polymerization, in order to enlarge the amorphous region and PP transformed from a resin to a particle with surface micropores. The swelling effect could not only expand the amorphous region further but also enabled the BPO initiator and AA and MAH monomers to diffuse through the surface and into the pores of PP particles more uniformly. Especially, under the action of xylene, they could migrate to the internal micropores of PP more conveniently.

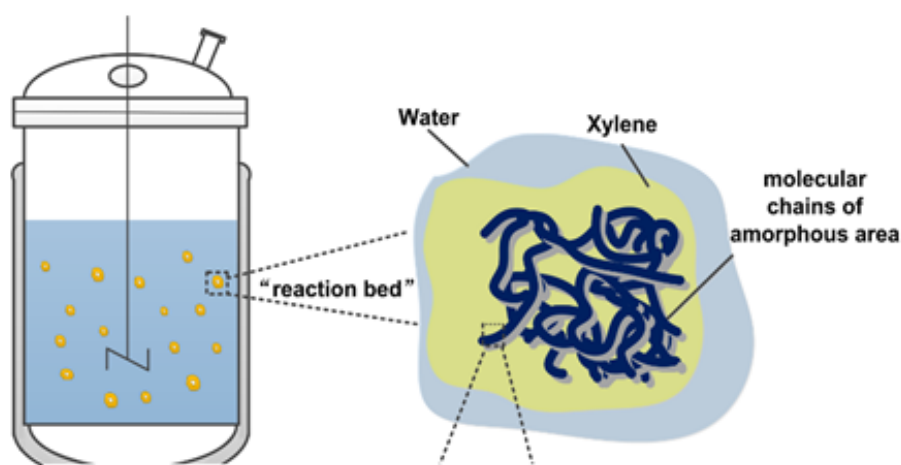
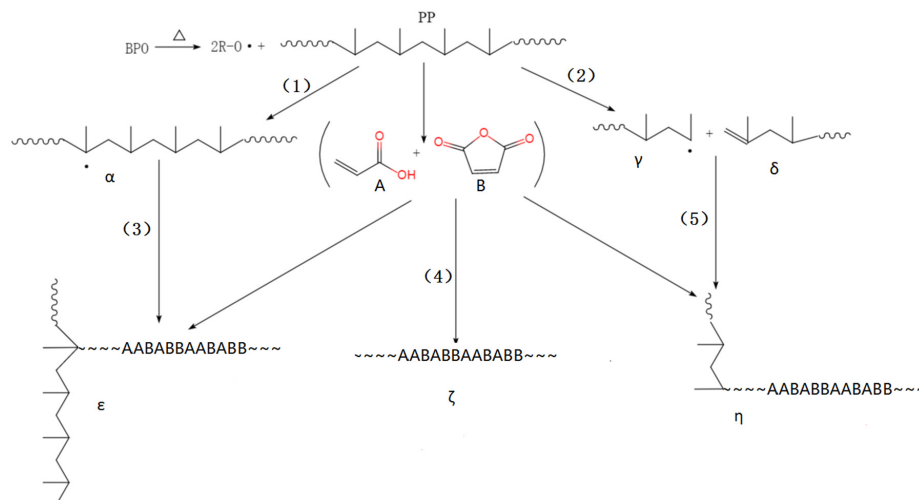


Figure 2. The suspension grafting reaction system.



**Figure 3.** The mechanism of suspension grafting polymerization of AA and MAH monomers.

Generally, the initiator first decomposes to form primary free radicals. The primary free radicals can generate PP macromolecular free radicals denoted as  $\alpha$ , by capturing  $\alpha$ -H from the PP molecular chains (Reaction 1). The macromolecular free radicals,  $\alpha$ , react with monomers to form the target product,  $\epsilon$  (Reaction 3). However, side reactions like homo-polymerization of monomers (Reaction 4) and PP degradation (Reaction 2), also occur during this process. In the presence of AA, AA first attacks the PP macromolecular radicals  $\alpha$  during the grafting polymerization, since AA is an electron provider and has higher reactivity. It can rapidly react with the PP macromolecular radicals  $\alpha$ . Moreover, it inhibits side reactions like degradation to form stable PP-AA macromolecular free radicals. The macromolecular free radicals further react with AA or MAH, which is the main reaction pathway. At the same time, due to low reaction temperature, it becomes difficult for the degradation products to react with the monomer (Reaction 5).

### 3.2. Effect of Quenching Treatment

The PP used in this research is a special raw material for melt-blown process. It has high crystallinity, but the suspension grafting modification is mainly carried out in the amorphous regions of PP. Therefore, the PP melt can be quenched to reduce its crystallinity, which makes the grafting polymerization easier. It can be seen from the X-ray diffraction patterns of PP before and after the quenching treatment in Figure 4 that the dispersion peak intensity (shaded area in the figure) of the amorphous region of the quenched PP was significantly greater than that of the original PP. Since the quenching process greatly shortens the crystallization time of the PP melt, some of the PP macromolecular chains have no time to move, transform from the disordered coils and then grow into crystals, which results in lower crystallinity.

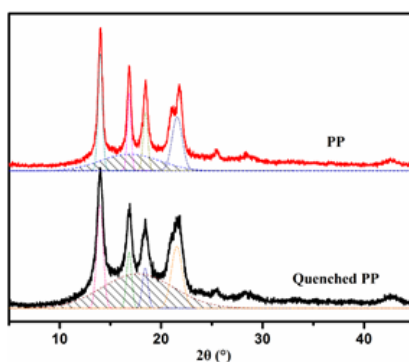


**Figure 4.** X-ray diffraction patterns of PP before and after the quenching treatment.

### 3.3. Effects of Different Parameters on Grafting Ratio in Suspension Grafting Polymerization

The main factors affecting grafting in suspension grafting polymerization include the grafting time, the AA/MAH ratio, the total amount of monomers, and the dosages of BPO, xylene, and deionized water. Therefore, effects of the six factors on the grafting ratio were all investigated and the results are shown in Figure 5.

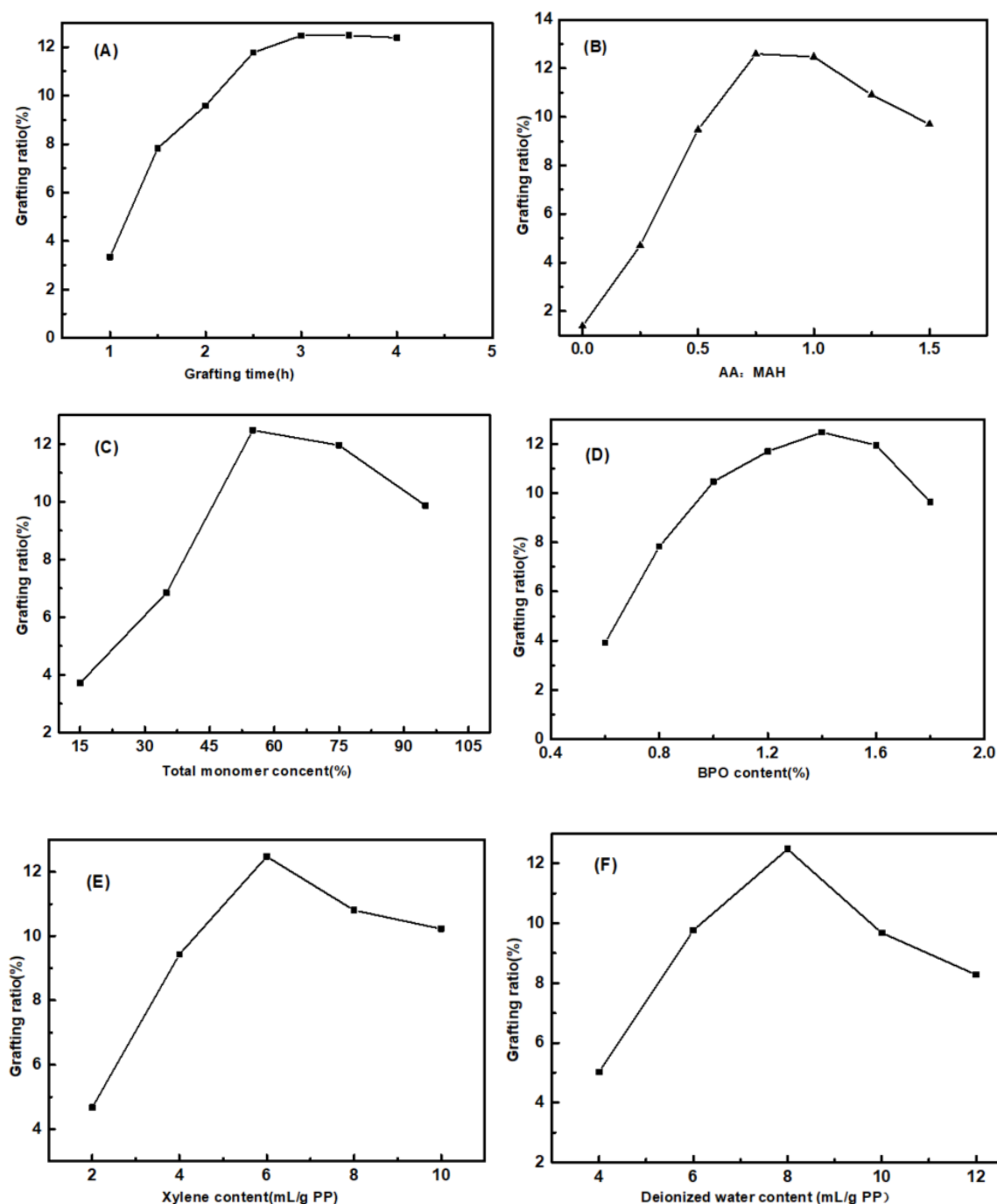


**Figure 5.** Effects of grafting time (A), AA/MAH ratio (B), total monomer content (C), and the dosages of BPO (D), xylene (E), and deionized water (F) on grafting ratio.

It can be seen from Figure 5A that the grafting ratio increased rapidly with increase in grafting time and it reached a stable state after three hours. The half-life period of the initiator BPO at 90 °C is 1 h [29]. In the initial stages of the reaction, BPO decomposed into a large number of primary free

radicals, which rapidly initiated the grafting reaction. In addition, the monomer concentration was also high at this time, due to which the grafting ratio increased rapidly. After 3 h, BPO was basically decomposed and the monomer concentration was also lower, exhibiting a more stable grafting ratio.

From Figure 5B, it is evident that when the mass fraction of AA was 0, the grafting ratio was only 1.38%. Subsequently, as the AA/MAH ratio increased, the grafting ratio increased at first and then decreased. With increase in the amount of monomer AA added, the concentration of macromolecular free radicals with AA chains increased. This increased the probability of free radicals contacting with PP. In addition, the monomer MAH could not undergo self-polymerization, due to its steric hindrance. When AA was added, it could form a copolymer with MAH and then graft with the PP segment [38], due to which the grafting ratio increased. However, as the amount of AA added continued to increase, the probability of capturing primary free radicals increased, thereby forming a greater number of AA-containing macromolecular free radicals. The probability of termination due to recombination between these free radicals increased, which resulted in lower grafting ratio. In addition, more the number of AA molecules, more was the probability of AA initiation, which then reduced the probability of formation of macromolecular free radicals of PP, thereby affecting the grafting ratio.

It can be seen from Figure 5C that as the total amount of monomers AA and MAH increased, the grafting ratio increased at first and then decreased. Higher monomer concentration increased the effective collisions between the monomers and PP macromolecular radicals, thereby increasing the grafting ratio. However, grafting polymerization mainly occurred in the amorphous regions of PP. Although the amorphous regions of PP expanded after quenching, the reaction space was still limited. Too high monomer concentration led to more homopolymerization as the side reaction. Additionally, the mass transfer of monomer and initiator were also affected, so the grafting ratio decreased.

With an increase in the amount of initiator BPO, the grafting ratio first increased and then decreased. When the amount of added BPO accounted for 1.4% of PP, the grafting ratio reached the maximum value of 12.47% (Figure 5D). On heating, BPO first decomposed into benzoyl radicals. Due to steric hindrance, benzoyl radicals were further decomposed into benzene radicals with stronger capability for H atom. Benzene radicals flowed and diffused slowly in the PP particles within limited space, depriving the  $\alpha$ -H from the PP chains to form PP macromolecular radicals and initiating monomer polymerization. Therefore, by appropriately increasing the amount of BPO, a greater number of benzene radicals could be generated. This increased the number of monomers participating in the grafting reaction and increased the grafting ratio. However, excessively high concentration of benzene radicals could cause explosive polymerization and lead to an increase in homopolymerization side reactions. This would again affect the progress of the grafting reaction and also result in degradation of PP [39].

It can be seen from Figure 5E that, with the increase in amount of xylene, the grafting ratio increased rapidly and then decreased slightly. With xylene concentration of 6 mL/g PP, the grafting ratio reached the maximum value of 12.47%. The monomers used in this study possessed polar groups, and hence their solubility parameters were quite different from that of PP, which implied lower swelling capability of PP. The addition of certain amount of xylene helped to increase the swelling degree of PP and provided greater space for the grafting reaction. Meanwhile, the addition of xylene also kept the concentration of water-soluble monomers at the interface to a low level. This effectively reduced homo-polymerization as side reaction and increased the grafting ratio. However, too much xylene readily formed a film covering the surface of PP, which hindered the grafting reaction between monomer and PP and affected the grafting ratio.

Figure 5F shows that as the amount of deionized water as dispersant increased, the grafting ratio increased rapidly and then decreased. As the amount of deionized water reached 8 mL/g PP, the grafting ratio reached the maximum value. If the amount of deionized water added was too less, the dispersion of PP into multiple independent "reaction beds" became difficult, since PP particles agglomerated in the reactor to form agglomerates, resulting in a low grafting ratio. With too much of deionized water, although the PP particles could form numerous independent "reaction beds",

the concentration of monomer dissolved in the water decreased. Hence, the monomer concentration gradient between the dispersion medium and the interfacial reaction layer became smaller. As a result, it was difficult for the monomer molecules to enter the interfacial layer and participate in the grafting polymerization reaction, due to which the grafting ratio decreased.

Based on the aforementioned study of the effect of parameters of suspension graft polymerization on the grafting rate, the optimal combination of parameters for suspension graft polymerization are presented in Table 1.

**Table 1.** The optimal combination of parameters for suspension graft polymerization.

PP	Monomers		Xylene	Deionized Water	BPO	Grafting Time	Grafting Ratio
	AA	MAH					
200 g	47 g	63 g	1.2 L	1.6 L	2.8 g	3 h	12.47%

### 3.4. Effect of Suspension Grafting on the Performance of Melt-Blown Spinning Product

Melt-blown spinning has strict requirements of fluidity and thermal stability of raw materials. PP resin itself has greater fluidity, but after its modification with polar groups, the interactions between molecular chains increase and the fluidity is affected. In addition, in the melt-blown spinning process, the raw materials are melted at high temperature and extruded through the screw. Hence, only better thermal stability can ensure that no decomposition of the raw materials occurs during the process. Therefore, the melt flow rate (MFR) and thermogravimetric (TG) of PP and PP-g-(AA-MAH) were investigated to determine whether it can be spun into fibers. The results are presented in Figure 6.

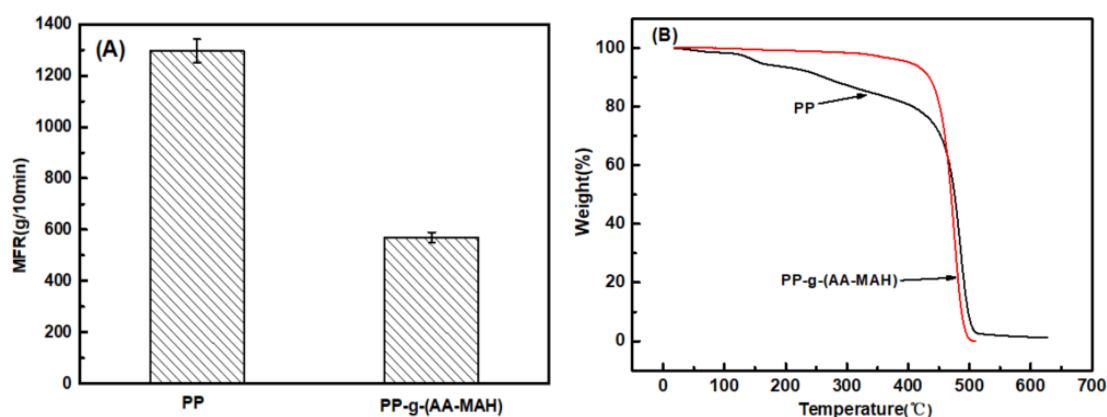


**Figure 6.** MFR (A) and TG (B) of PP and PP-g-(AA-MAH) fibers.

It can be seen from Figure 6A that MFR (570 g/10 min) of the product PP-g-(AA-MAH) of suspension grafting was lower than that of the PP raw material (1296 g/10 min), implying decrease in fluidity. However, the MFR was still higher than that required for the melt-blown process of PP melt (400 g/10 min). The decrease in MFR could be attributed mainly to the strengthening of hydrogen bonds between the grafted polar chains [29,34]. Compared with the TG curves of unmodified PP in Figure 6B, the product of suspension grafting PP-g-(AA-MAH) had better thermal stability. PP-g-(AA-MAH) showed no significant weight loss before 250 °C, and hence the melt-blown spinning at maximum temperature of 220 °C basically did not cause decomposition.

### 3.5. Characterization of Fibers

#### 3.5.1. Fourier Transform Infrared Analysis (FT-IR)

PP and its products of suspension grafting - PP-g-AA, PP-g-MAH, and PP-g-(AA-MAH) were spun by melt-blowing and processed into fibers. Their FTIR spectra (the total monomer contents

were the same during the suspension grafting process) are shown in Figure 7. The fibers of modified PP-g-AA, PP-g-MAH, and PP-g-(AA-MAH) showed unique characteristic absorption peaks of PP, viz. symmetrical ( $2924\text{ cm}^{-1}$ ) and asymmetrical ( $2842\text{ cm}^{-1}$ ) C-H stretching vibrations of  $-\text{CH}_3$ , the flexural vibrations of  $-\text{CH}_2-$  at  $1380\text{ cm}^{-1}$ , and absorption of C-H at  $1450\text{ cm}^{-1}$ . Compared with that of PP fiber, the FTIR spectrum of PP-g-AA fiber showed peak for C=O stretching vibrations of the carboxyl group ( $1720\text{ cm}^{-1}$ ), indicating the successful grafting of AA onto the PP chain. Compared to the spectrum of PP fiber, PP-g-MAH showed a peak at  $1780\text{ cm}^{-1}$ , which was attributed to the symmetric and asymmetric vibrations of C=O of acid anhydride. The peak at  $1720\text{ cm}^{-1}$  was ascribed to the C=O of carboxylic acid, formed by the hydrolysis of anhydride. The FTIR spectra of PP-g-(AA-MAH), PP-g-AA, and PP-g-MAH fibers all showed peaks for stretching vibrations of C=O of the carboxyl group at  $1720\text{ cm}^{-1}$ . The difference was that the FTIR spectrum of PP-g-(AA-MAH) had stronger intensity for C=O peak, indicating that its carboxyl content was higher than those of PP-g-AA and PP-g-MAH fibers. However, the FTIR spectrum of PP-g-(AA-MAH) fiber did not show peaks for symmetrical and asymmetrical vibrations of C=O of acid anhydride in the PP-g-MAH spectrum. This was due to the fact that MAH was grafted on to PP in the form of maleic acid [39,40]. FTIR results confirmed the successful grafting of AA and MAH onto PP fibers.

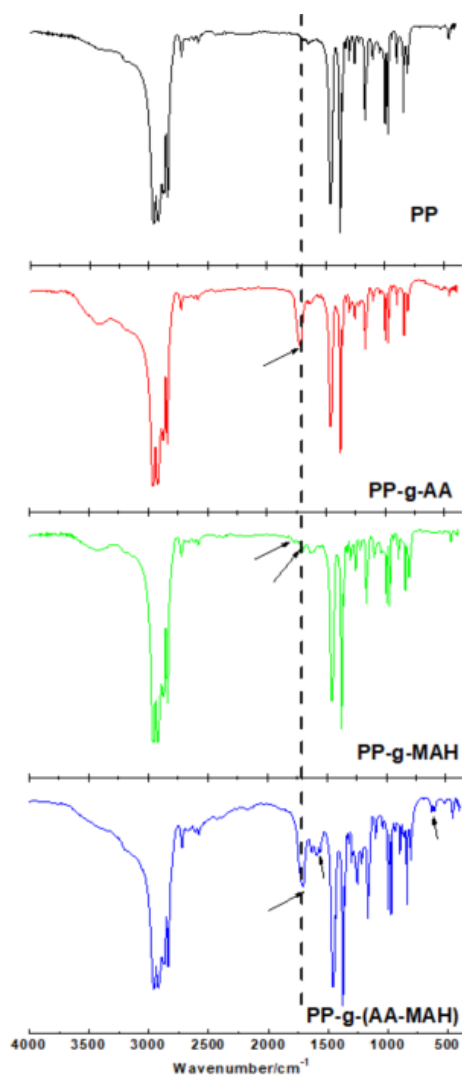


**Figure 7.** FTIR spectra of PP, PP-g-AA, PP-g-MAH and PP-g-(AA-MAH) fibers.

### 3.5.2. <sup>1</sup>H-NMR Analysis

The carboxyl group in PP-g-(AA-MAH) fiber was linked to –CH–. From the <sup>1</sup>H-NMR analysis (Figure 8), it was evident that compared with PP fiber, PP-g-(AA-MAH) fiber showed a chemical shift at around 2.3 ppm [41], indicating that the carboxyl groups were successfully grafted onto the surface of PP fibers.

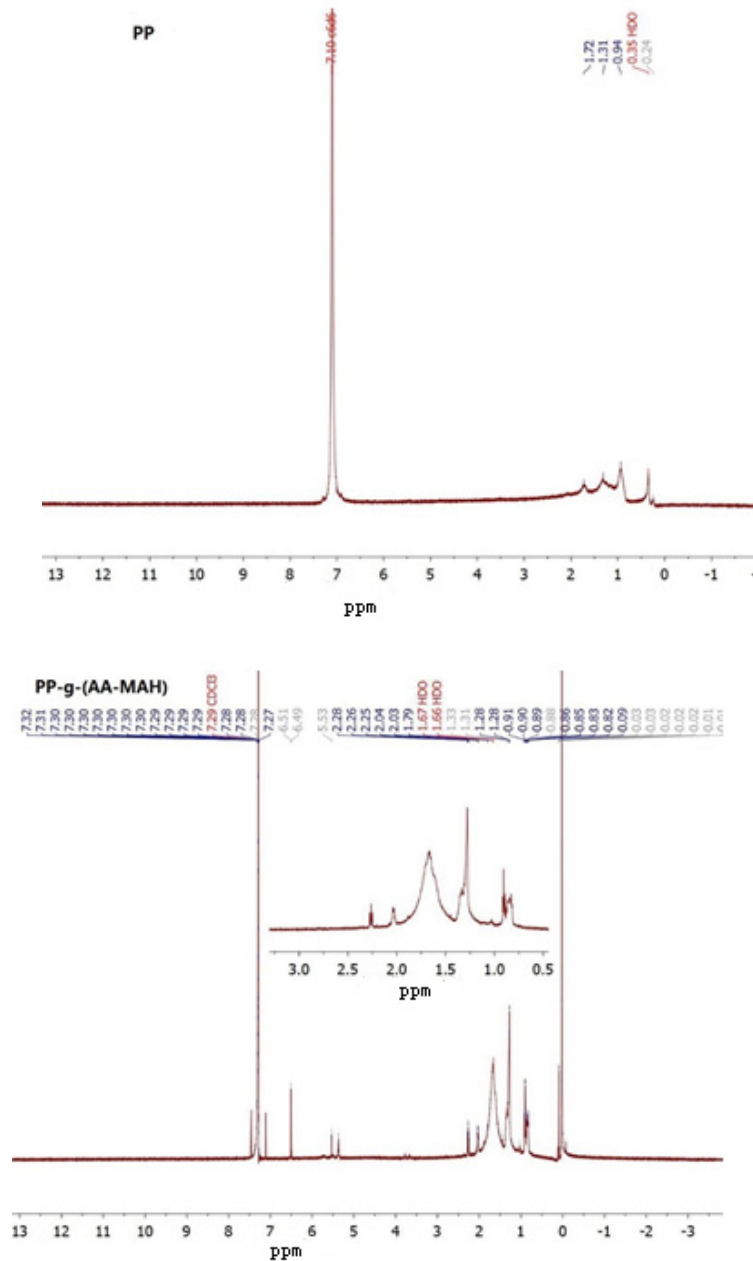
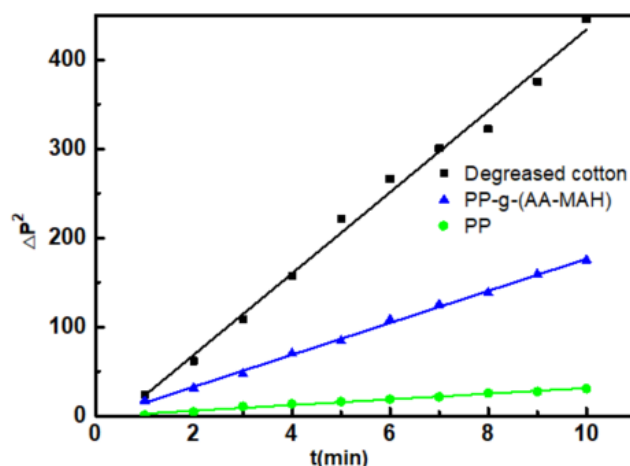


Figure 8. <sup>1</sup>H-NMR analysis of PP and PP-g-(AA-MAH) fibers.

### 3.5.3. Analysis on Hydrophilicity

Figure 9 showed a linear fitting relationship of  $(\Delta P)^2$  of degreased cotton, PP-g-(AA-MAH) fiber and PP fiber with  $t$ . It could be seen from the figure that the  $K_0$  of degreased cotton was 45.66, whereas  $K_0$  of PP-g-(AA-MAH) fiber and PP fiber were 17.95 and 3.19, respectively. According to Equation (4), the calculated water contact angles of PP-g-(AA-MAH) fiber and PP fiber were 66.85° and 85.98°, respectively, which indicated increased hydrophilicity of PP-g-(AA-MAH) fibers.



**Figure 9.** Linear fitting relationship of  $(\Delta P)^2$  of degreased cotton, PP-g-(AA-MAH) and PP fiber with  $t$ .

### 3.6. Investigation of Aniline-Adsorption Performance of PP-g-(AA-MAH) Fiber before and after Regeneration

#### 3.6.1. Effect of pH on the Adsorption Capacity

Solution pH value influences the surface properties of PP-g-(AA-MAH) fibers and the state of aniline in water, which in turn has an effect on the adsorption. Figure 10 shows the effect of pH value on the adsorption capacity of PP-g-(AA-MAH) fibers. The adsorption capacity first increased and then decreased in the pH range from 3 to 10. The adsorption capacity reached the maximum value of 48.3 mg/g, when the solution was neutral.

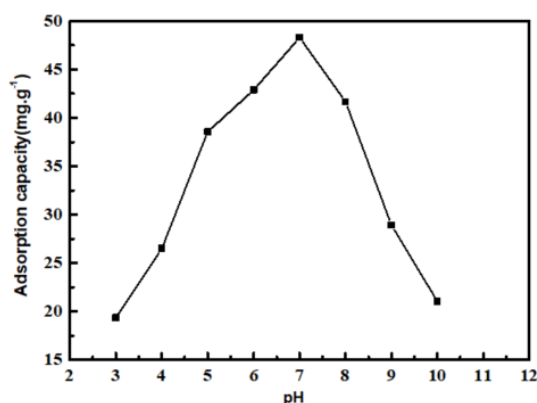


**Figure 10.** The effect of the pH value on the adsorption capacity.

Aniline is weakly alkaline and has  $pK_b$  value (dissociation constant) of 9.4. In other words, aniline exists as  $C_6H_5NH_3^+$  below 9.4 pH and in molecular form above 9.4 pH [20,21]. Combining this with the point of zero charge (3.02) of the PP-g-(AA-MAH) fiber in the aqueous solution (from Figure 11), the surface of PP-g-(AA-MAH) fiber was protonated and positively charged below 3.02. Therefore, the electrostatic repulsion between aniline (in the form of  $C_6H_5NH_3^+$ ) and positively charged surface led to its poor adsorption. Above 3.02, the surface of PP-g-(AA-MAH) fiber was negatively charged due to deprotonation. The number of  $-COO^-$  groups on the surface increased and the electrostatic attraction was strengthened. Hence, the adsorption capacity of PP-g-(AA-MAH) fibers towards aniline gradually increased between pH 3~7. As pH value continued to rise and the aqueous solution turned alkaline, the reduction of  $C_6H_5NH_3^+$  led to the reductions in adsorption capacity, although the number of  $-COO^-$  groups increased. Above pH 9.4, aniline mainly existed in the molecular form and had lower solubility, which was not conducive for adsorption, and hence the adsorption capacity decreased further.

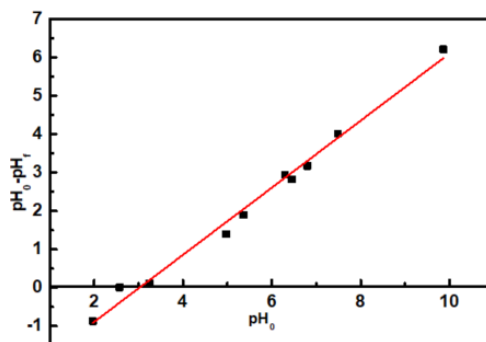


Figure 11. The point of zero charge of PP-g-(AA-MAH) fiber in the aqueous solution.

### 3.6.2. Adsorption Kinetics

Under the conditions of 25 °C, pH = 7, and initial aniline concentration of 300 mg/L, the adsorptivities of aniline on PP-g-(AA-MAH) fibers at different adsorption times were investigated, and the kinetics was studied, as shown in Figure 12. Figure 12A showed that PP-g-(AA-MAH) fibers had faster adsorptivity for aniline within the first 45 min, with adsorption capacity reaching up to 42.2 mg/g. Then, the adsorption capacity increased slowly until it reached saturation as 48.3 mg/g at 120 min. The faster rate of adsorption within the first 45 min was the result of the large number of active sites on the surface of PP-g-(AA-MAH) fibers. With the prolongation of adsorption time, the number of active sites on the surface of PP-g-(AA-MAH) fibers gradually decreased along with decrease in aniline concentration. As a result, the driving force for adsorption obviously weakened and the adsorption capacity increased slowly until it reached saturated adsorption. From the linear fitting results (Figure 12B,C), The  $R^2$  of the pseudo-first-order kinetic model is 0.9734, while for the pseudo-second-order kinetic model,  $R^2$  is 0.9955. Hence, the adsorption for aniline is better fitted by the pseudo-second-order kinetic model, indicating that the adsorption is controlled by chemical phenomena [42]. Hence, the electrostatic attraction is the main driving force for aniline adsorption on PP-g-(AA-MAH) fibers.

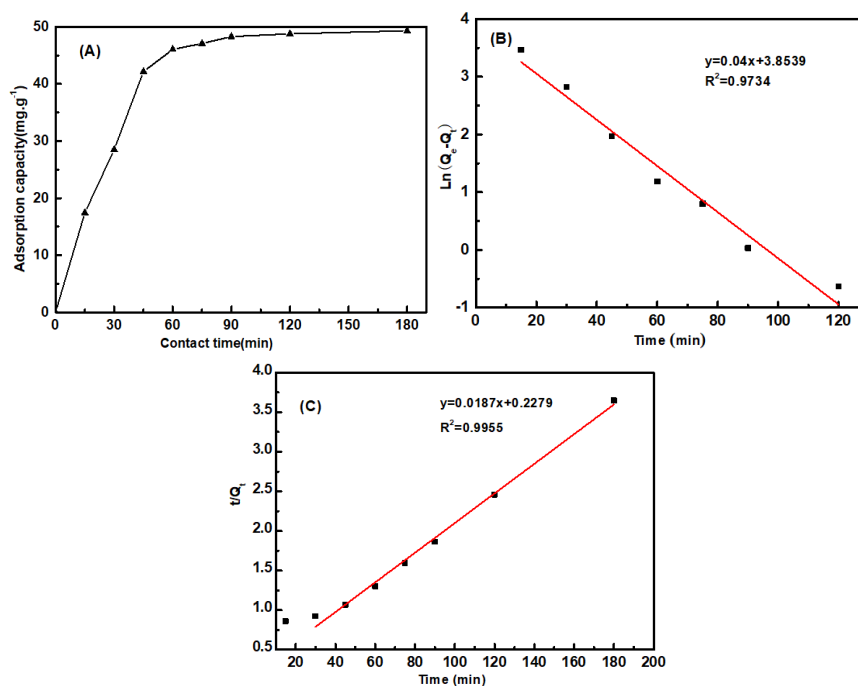
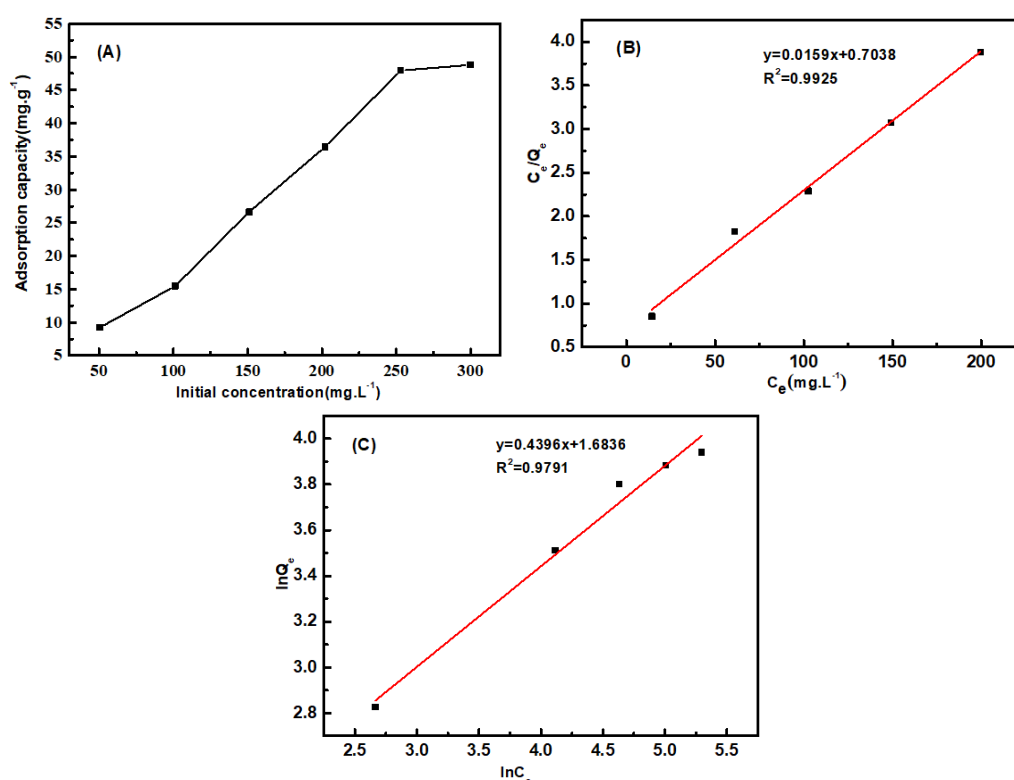


Figure 12. The effect of contact time on adsorption capacity (A) and the linearized pseudo-first-order (B) and pseudo-second-order (C) kinetics.

### 3.6.3. Adsorption Isotherm

The adsorption isotherm was drawn based on the results obtained using different initial aniline concentrations. As can be seen from Figure 13A, the adsorption capacity increased with the increase in initial aniline concentration, and eventually became stable. With the increase in aniline concentration, the probability of collision between functional groups on fibers and aniline increased, and so the adsorption capacity increased. However, the number of functional groups was limited, and the adsorption capacity eventually tended to be stable. The linearized versions of the two models are illustrated in Figure 13B,C and the values of the isotherm parameters are listed in Table 2. It was found that the  $R^2$  value of Langmuir and Freundlich was 0.9925 and 0.9791, respectively, and the adsorption for aniline of PP-g-(AA-MAH) fibers is better fitted by the Langmuir model. The uptake of aniline occurs on the homogeneous surface of PP-g-(AA-MAH) fibers by monolayer adsorption. The maximum theoretical adsorption capacity for aniline of PP-g-(AA-MAH) fibers is 62.7 mg/g.



**Figure 13.** The effect of initial aniline concentration on adsorption capacity (A) and the linearized Langmuir(B) and Freundlich (C) models.

**Table 2.** Isotherm parameters.

Langmuir			Freundlich		
$Q_m/\text{mg}\cdot\text{g}^{-1}$	$K_L$	$R^2$	$n$	$K_F/\text{mg}\cdot\text{g}^{-1}$	$R^2$
62.7	0.0226	0.9925	2.2745	5.3851	0.9791

### 3.6.4. Comparison of Adsorption Capacity with other Adsorbents

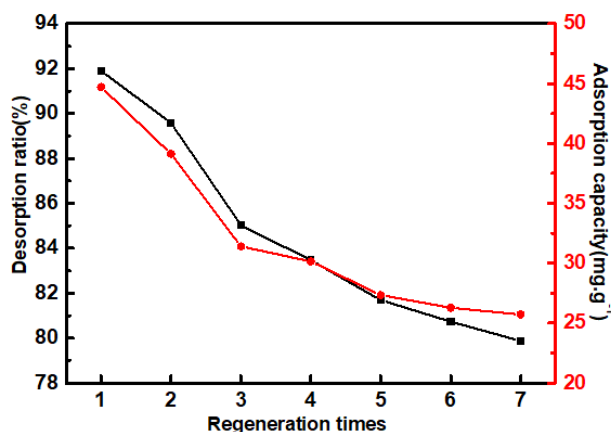
Comparisons between maximum adsorption capacities ( $q_{\max}$ ) of PP-g-(AA-MAH) fibers and other adsorbents for aniline reported in the literature are presented in Table 3. The results show that PP-g-(AA-MAH) fibers exhibits a reasonable capacity for aniline adsorption.

**Table 3.** Adsorption capacity of various adsorbents for aniline

Adsorbents	$q_{\max}/\text{mg}\cdot\text{g}^{-1}$	Reference
Modified pine sawdust	21.8	[43]
Activated carbon/chitosan composite	22.9	[44]
PAM/SiO <sub>2</sub>	52.0	[45]
Modied ATP	16.1	[46]
Cr-bentonite	21.6	[47]
Modified jute fiber	125	[20]
Edible fungus residue activated carbon	27.1	[21]
PP-g-(AA-MAH) fibers	48.3	This work

### 3.6.5. Desorption and Regeneration

The regeneration performance of PP-g-(AA-MAH) fibers was investigated using the desorption ratio and adsorption capacity of regenerated fiber, as shown in Figure 14. It can be seen that after seven adsorption-desorption cycles, the desorption ratio of the PP-g-(AA-MAH) fiber still remained above 80% and the adsorption capacity for aniline could still reach 25.72 mg/g, indicating that PP-g-(AA-MAH) fiber had good regeneration-adsorption performance.

**Figure 14.** The desorption ratio and adsorption capacity of regenerated fiber.

## 4. Conclusions

With PP as the matrix, AA and MAH as functional monomers, PP-g-(AA-MAH) fiber was prepared by suspension grafting and melt-blown spinning technology. The technology can be easily scaled-up to industrial level and the fibers can be used to adsorb aniline. The maximum grafting ratio was 12.47% under the following optimal suspension grafting conditions: grafting time of 3 h, AA: MAH = 0.75, total monomer content of 55%, BPO content of 1.4%, xylene content of 6 mL/g PP, and deionized water content of 8 mL/g PP. Melt flow-rate and thermal analysis indicated that the suspension grafting product had good fluidity and thermal stability, and could be spun by melt-blown process. FTIR and NMR analyses showed that AA and MAH were successfully grafted onto PP fibers. The hydrophilicity of PP-g-(AA-MAH) fiber was enhanced. Therefore, the adsorption for aniline from aqueous solution was fast and the adsorption capacity could reach up to 42.2 mg/g at 45 min and pH = 7. The kinetics of adsorption followed the pseudo-second-order model and the adsorption isotherm data were better fitted by the Langmuir model. Moreover, the fibers had good regeneration performance.

**Author Contributions:** Conceptualization, Z.L. (Zhouyang Lian) and W.W.; Data curation, J.Z., H.Q. and Z.L. (Zhengwei Luo); Formal analysis, H.Q. and Z.L. (Zhengwei Luo); Investigation, Y.X. and J.Z.; Methodology, Z.L. (Zhouyang Lian), Y.X., H.Q. and W.W.; Writing—original draft, Z.L. (Zhouyang Lian), H.Q., Z.L. (Zhengwei Luo) and W.W.; Writing—review & editing, Z.L. (Zhouyang Lian). All authors have read and agreed to the published version of the manuscript.

**Funding:** This work was financially supported by the National Natural Science Foundation of China (Grant Number 21676144).

**Acknowledgments:** W.W. would like to thank the support from the Natural Science Foundation of China (Grant Number 21676144).

**Conflicts of Interest:** The authors declare no conflict of interest.

## References

1. Pagalan, E.; Sebron, M. Activated carbon from spent coffee grounds as an adsorbent for treatment of water contaminated by aniline yellow dye. *Ind. Crops Prod.* **2020**, *145*, 111953. [CrossRef]
2. Reddy, M.C.S.; Nirmala, V. Bengal Gram Seed Husk as an adsorbent for the removal of dye from aqueous solutions—Batch studies. *Arab. J. Chem.* **2017**, *10*, S2554–S2566. [CrossRef]
3. Ferreiro, C.; Villota, N. An efficient catalytic process for the treatment of genotoxic aniline wastewater using a new granular activated carbon-supported titanium dioxide composite. *J. Clean. Prod.* **2019**, *228*, 1282–1295. [CrossRef]
4. Koyuncu, H.; Kul, A.R. Removal of aniline from aqueous solution by activated kaolinite: Kinetic, equilibrium and thermodynamic studies. *Colloids Surf. A Physicochem. Eng. Asp.* **2019**, *569*, 59–66. [CrossRef]
5. Dewage, N.B.; Liyanage, A.S. Fast aniline and nitrobenzene remediation from water on magnetized and nonmagnetized Douglas fir biochar. *Chemosphere* **2019**, *225*, 943–953. [CrossRef]
6. Qi, Y.G.; Toyooka, T. Comparative  $\gamma$ -H2AX analysis for assessment of the genotoxicity of six aromatic amines implicated in bladder cancer in human urothelial cell line. *Toxicol. In Vitro* **2020**, *66*, 104880. [CrossRef]
7. Tao, N.; Liu, G.Y. Genotoxicity and growth inhibition effects of aniline on wheat. *Chemosphere* **2017**, *169*, 467–473. [CrossRef]
8. Eskola, M.; Altieri, A. Overview of the activities of the European food safety authority on mycotoxins in food and feed. *World Mycotoxin J.* **2018**, *11*, 277–289. [CrossRef]
9. European Commission. *European Union Risk Assessment Report Aniline*; Office for Official Publications of the European Communities: Luxembourg, 2004.
10. US EPA Organization. Contaminant Candidate List 4-CCL 4. US EPA, 2014. Available online: <https://www.epa.gov/ccl/contaminant-candidate-list-4-ccl-4-0> (accessed on 10 September 2018).
11. Gang, X.; Wang, Q. Simultaneous removal of aniline, antimony and chromium by ZVI coupled with H<sub>2</sub>O<sub>2</sub>: Implication for textile wastewater treatment. *J. Hazard. Mater.* **2019**, *368*, 840–848.
12. Qi, Y.F.; Guo, C. Co/Fe and Co/Al layered double oxides ozone catalyst for the deep degradation of aniline: Preparation, characterization and kinetic model. *Sci. Total Environ.* **2020**, *715*, 136982. [CrossRef]
13. Li, W.; Chen, C. Efficient removal of aniline by micro-scale zinc-copper (mZn/Cu) bimetallic particles in acidic solution: An oxidation degradation mechanism via radicals. *J. Hazard. Mater.* **2019**, *366*, 482–491. [CrossRef] [PubMed]
14. Dvorak, L.; Lederer, T. Removal of aniline, cyanides and diphenylguanidine from industrial wastewater using a full-scale moving bed biofilm reactor. *Process Biochem.* **2014**, *49*, 102–109. [CrossRef]
15. Gomez, J.L.; Leon, G. Application of reverse osmosis to remove aniline from wastewater. *Desalination* **2009**, *245*, 687–693. [CrossRef]
16. Wu, X.H.; Lei, Z.G. Liquid–liquid extraction of low-concentration aniline from aqueous solutions with salts. *Ind. Eng. Chem. Res.* **2010**, *49*, 2581–2588. [CrossRef]
17. Li, C.H. Recovery of aniline from wastewater by nitrobenzene extraction enhanced with salting-out effect. *Biomed. Environ. Sci.* **2010**, *23*, 208–212. [CrossRef]
18. Zhang, Q.; Zhang, W.L. Effects of dissolved oxygen concentrations on a bioaugmented sequencing batch reactor treating aniline-laden wastewater: Reactor performance, microbial dynamics and functional genes. *Bioresour. Technol.* **2020**, *313*, 123598. [CrossRef]
19. Gan, Y.; Chen, G. Oxygen-rich hyper-cross-linked polymers with hierarchical porosity for aniline adsorption. *Chem. Eng. J.* **2019**, *368*, 29–36. [CrossRef]
20. Gao, D.W.; Hu, Q. High-capacity adsorption of aniline using surface modification of lignocellulose-biomass jute fibers. *Bioresour. Technol.* **2015**, *193*, 507–512. [CrossRef]

21. Li, H.Y.; Liu, L.X. High-efficiency adsorption and regeneration of methylene blue and aniline onto activated carbon from waste edible fungus residue and its possible mechanism. *RSC Adv.* **2020**, *10*, 14262–14273. [[CrossRef](#)]
22. Huang, Q.; Hu, D.W. Sequential removal of aniline and heavy metal ions by jute fiber biosorbents: A practical design of modifying adsorbent with reactive adsorbate. *J. Mol. Liq.* **2019**, *285*, 288–298. [[CrossRef](#)]
23. Chang, Y.; Ren, C. Preparation and characterization of Fe<sub>3</sub>O<sub>4</sub>/graphene nanocomposite and investigation of its adsorption performance for aniline and p-chloroaniline. *Appl. Surf. Sci.* **2012**, *261*, 504–509. [[CrossRef](#)]
24. Sajab, M.S.; Chia, C.H. Cationic and anionic modifications of oil palm empty fruit bunch fibers for the removal of dyes from aqueous solutions. *Bioresour. Technol.* **2013**, *128*, 571–577. [[CrossRef](#)]
25. Chai, W.B.; Liu, X.Y. Preparation and characterization of polypropylene fiber-grafted polybutylmethacrylate as oil sorbent. *Desalin. Water Treat.* **2016**, *57*, 18560–18571. [[CrossRef](#)]
26. Mahtabani, A.; Rytoluoto, I. On the Silica Surface Modification and Its Effect on Charge Trapping and Transport in PP-Based Dielectric Nanocomposites. *ACS Appl. Polym. Mater.* **2020**, *2*, 3148–3160. [[CrossRef](#)]
27. Soylemez, M.A.; Barsbay, M. Preparation of well-defined erythromycin imprinted non-woven fabrics via radiation-induced RAFT-mediated grafting. *Radiat. Phys. Chem.* **2018**, *142*, 77–81. [[CrossRef](#)]
28. Luo, Z.W.; Chen, H.N. Surface grafting of styrene on polypropylene by argon plasma and its adsorption and regeneration of BTX. *J. Appl. Polym. Sci.* **2018**, *135*, 46171. [[CrossRef](#)]
29. Guo, M.L.; Zhang, C. An Efficient, Simple and Facile Strategy to Synthesize Polypropylene-g-(acrylic acid-co-acrylamide) Nonwovens by Suspension Grafting Polymerization and Melt-blown Technique. *Fibers Polym.* **2016**, *17*, 1123–1130. [[CrossRef](#)]
30. Luo, Z.W.; Xu, J.H. Ion-Imprinted Polypropylene Fibers Fabricated by the Plasma-Mediated Grafting Strategy for Efficient and Selective Adsorption of Cr(VI). *Polymers* **2019**, *11*, 1508. [[CrossRef](#)]
31. Chen, H.N.; Guo, M.L. Green and Efficient Synthesis of an Adsorbent Fiber by Plasma-induced Grafting of Glycidyl Methacrylate and Its Cd(II) Adsorption Performance. *Fibers Polym.* **2018**, *19*, 722–733. [[CrossRef](#)]
32. Liang, F.C.; Yuan, H. Study of suspension grafting process of polypropylene. *Des. Monomers. Polym.* **2018**, *21*, 130–136. [[CrossRef](#)]
33. Li, Z.; Ma, Y.H. A Facile, Green, Versatile Protocol to Prepare Polypropylene-g-Poly(methyl methacrylate) Copolymer by Water-Solid Phase Suspension Grafting Polymerization Using the Surface of Reactor Granule Technology Polypropylene Granules as Reaction Loci. *J. Appl. Polym. Sci.* **2013**, *129*, 3170–3177. [[CrossRef](#)]
34. Kyung, B.I.; Young, K.H. Development of a Melt-blown Nonwoven Filter for Medical Masks by Hydro Charging. *Text. Sci. Eng.* **2014**, *51*, 186–192.
35. Ji, L.Y.; Shi, B.L. A novel method for determining surface free energy of powders using Washburn's equation without calculating capillary factor and contact angle. *Powder Technol.* **2015**, *271*, 88–92. [[CrossRef](#)]
36. Chang, Q.; Wei, B.G. Capillary pressure method for measuring lipophilic hydrophilic ratio of filter media. *Chem. Eng. J.* **2009**, *150*, 323–327.
37. Chen, M.; Ding, W.H. Removal of azo dyes from water by combined techniques of adsorption, desorption, and electrolysis based on a supramolecular sorbent. *Ind. Eng. Chem. Res.* **2013**, *52*, 2403–2411. [[CrossRef](#)]
38. Wu, R.D.; Tong, X.L. Grafting PP by Swelling Suspension Copolymerization Process. *China Plast.* **2002**, *8*, 64–68.
39. Wu, R.D.; Tong, X.L. Graft Copolymerization of Acrylic Acid onto Polypropylene by Suspension process. *J. Funct. Polym.* **2001**, *14*, 85–89.
40. Zhou, Q.; Yang, P.D. Preparation of PP-g-MAH fiber using suspension grafting and its adsorption ability for copper ions in water. *New Chem. Mater.* **2015**, *43*, 240–243.
41. Liang, T.; Yan, K. Synthesis of a low-molecular-weight copolymer by maleic acid and acrylic acid and its application for the functional modification of cellulose. *Cellulose* **2020**, *27*, 5665–5675. [[CrossRef](#)]
42. Wu, S.; Dai, X. Highly sensitive and selective ion-imprinted polymers based on one-step electrodeposition of chitosan-graphene nanocomposites for the determination of Cr(VI). *Carbohydr. Polym.* **2018**, *195*, 199–206. [[CrossRef](#)]
43. Zhou, Y.; Gu, X. Removal of aniline from aqueous solution using pine sawdust modified with citric acid and b-cyclodextrin. *Ind. Eng. Chem. Res.* **2014**, *53*, 887–894. [[CrossRef](#)]
44. Huang, R.; Yang, B. Simultaneous adsorption of aniline and Cr(VI) ion by activated carbon/chitosan composite. *J. Appl. Polym. Sci.* **2014**, *131*, 39903. [[CrossRef](#)]

45. An, F.; Feng, X. Adsorption of aniline from aqueous solution using novel adsorbent PAM/SiO<sub>2</sub>. *Chem. Eng. J.* **2009**, *151*, 183–187. [[CrossRef](#)]
46. Deng, Q.; Chen, C. Adsorption of aniline from aqueous solution using graphene oxide-modified attapulgite composites. *RSC Adv.* **2018**, *8*, 23382–23389. [[CrossRef](#)]
47. Zheng, H.; Liu, D. Sorption isotherm and kinetic modeling of aniline on Cr-bentonite. *J. Hazard. Mater.* **2009**, *167*, 141–147. [[CrossRef](#)] [[PubMed](#)]



© 2020 by the authors. Licensee MDPI, Basel, Switzerland. This article is an open access article distributed under the terms and conditions of the Creative Commons Attribution (CC BY) license (<http://creativecommons.org/licenses/by/4.0/>).